

Vision-Conditioned Variational Bayesian Last Layer Dynamics Models

Paul Brunzema¹, Thomas Lew², Ray Zhang², Takeru Shirasawa², John Subosits², Marcus Greiff^{2,*}

Abstract— Agile control of robotic systems often requires anticipating how the environment affects system behavior. For example, a driver must perceive the road ahead to anticipate available friction and plan actions accordingly. Achieving such proactive adaptation within autonomous frameworks remains a challenge, particularly under rapidly changing conditions. Traditional modeling approaches often struggle to capture abrupt variations in system behavior, while adaptive methods are inherently reactive and may adapt too late to ensure safety. We propose a vision-conditioned variational Bayesian last-layer dynamics model that leverages visual context to anticipate changes in the environment. The model first learns nominal vehicle dynamics and is then fine-tuned with feature-wise affine transformations of latent features, enabling context-aware dynamics prediction. The resulting model is integrated into an optimal controller for vehicle racing. We validate our method on a Lexus LC500 racing through water puddles. With vision-conditioning, the system completed all 12 attempted laps under varying conditions. In contrast, all baselines without visual context consistently lost control, demonstrating the importance of proactive dynamics adaptation in high-performance applications.

Video: <https://youtu.be/m-gcFK0moI8>.

I. INTRODUCTION

Accurate dynamics models are key to agile robotic autonomy, such as in scenarios like emergency avoidance or racing, where vehicles operate at the limits of handling [1]. At these extremes, even minor modeling errors can cascade into catastrophic failure [2], [3], making precise prediction of vehicle behavior essential for both safety and performance.

Traditional vehicle dynamics models rely on simplified assumptions about road conditions and tire behavior [4]–[6]. These assumptions hold in nominal settings but often fail when faced with significant environmental variations, especially when driving at the limit. For example, transitioning between dry and wet pavement significantly alters friction, leading to substantially different vehicle dynamics [7]. Learning-based approaches seek to compensate for such effects using online adaptation of a learned dynamics model [2], [8]–[11]. However, adaptation is reactive and often too slow to prevent instability near handling limits [2], motivating a shift toward anticipatory models that utilize exteroceptive sensing to adjust control strategies proactively.

While recent learned models achieve strong performance using proprioceptive data [2], [7], [8], [12], they are often blind to the environmental context. Incorporating exteroceptive cues from vision promises a shift from reactive to anticipatory

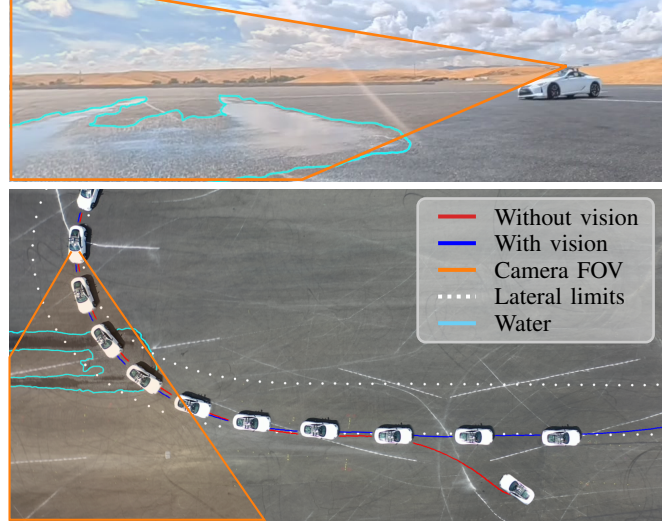


Fig. 1. A learned vehicle model conditioned on visual context is used for predictive control. With the visual context (orange), the car autonomously races through the water (blue), while models void of context spin out (red).

dynamics modeling. To this end, we introduce VcVBLL, a vision-conditioned variational Bayesian last-layer (VBLL) dynamics model. This novel model integrates visual context, extracted from forward-facing cameras, directly into the VBLL dynamics representation. The learned conditioning on visual information allows a controller to proactively adjust its actions before encountering challenging conditions. While this letter emphasizes racing as a challenging problem, the proposed concepts readily generalize to other applications.

Contributions. We propose a vision-conditioned VBLL dynamics (VcVBLL) model to capture changing vehicle dynamics arising from varying road surface properties (e.g., wet vs. dry conditions) through visual information. Specifically:

- With VcVBLL we present the first VBLL-based dynamics model conditioned on visual information. To address the scarcity of data with environmental changes (e.g., water-tire interactions), we introduce a two-stage fine-tuning procedure. This approach modulates the dynamics representation of a base VBLL trained on nominal driving data with a vision-conditioning path learned from limited wet-surface data. The resulting model yields interpretable adjustments in the predictive distribution.
- We integrate the VcVBLL dynamics model within a model predictive control (MPC) framework to achieve proactive, vision-informed autonomous racing on a Lexus LC500 in hardware experiments. Our model enables high-speed autonomous racing through changing conditions where all proprioceptive-only baselines spin out.

* Corresponding author.

¹Paul Brunzema is with the department of Mechanical Engineering, Aachen University, Germany. Email: paul.brunzema@googlemail.com. Paul was with TRI when conducting this research.

²The remaining authors are with Toyota Research Institute, 4440 El Camino Real, CA, USA. Email: first.last@tri.global.

Organization. We review related work in Sec. II and present preliminaries on vehicle modeling and optimal control in Sec. III. The proposed VcVBL model is developed in Sec. IV and the main results are presented in Sec. V.

II. RELATED WORK

Autonomous Driving at the Limit. High-performance driving research has focused on vehicle modeling and optimal control for racing [1], [3], [13]–[16] and drifting [7], [8], [12], [17]. In these works, MPC [18] is used to track a reference trajectory using a first-principles vehicle model [4], [17], [19], [20], often refined via system identification [21] with a fixed parametric form [22], parameter estimation [3], or online adaptation [1]. To capture more complex dynamics, neural network (NN) [14] and Gaussian process [10], [23] models have been explored. Recent work also demonstrates that diffusion-generated parameters can enable complex drifting [7], albeit at a higher computational cost. Other approaches include Koopman-based models that lift dynamics into a higher-dimensional space of observables [9], [24]. Crucially, these approaches do not consider proactive adaptation of the dynamics model based on exteroceptive information. Still, parametric NNs offer a distinct advantage as a model class: their flexibility enables conditioning on visual cues via mechanisms like FiLM [25]. Such conditioning has proven effective in vision-based manipulation [26], motivating learning exteroceptive-informed NN features from data.

Bayesian Last-Layer Models. Bayesian last-layer (BLL) models extend parametric NNs with Gaussian last-layer weights [23], [27]–[30] as a light-weight Bayesian NN. They provide Gaussian predictive posteriors and have shown promise in drifting [31] and off-road driving [32]. Variational BLL (VBLL) models [33] jointly learn last-layer weights and noise via a variational objective, achieving promising results across various applications [33], [34]. Therefore, we adopt VBLLs as our base architecture, applying this state-of-the-art model class to dynamics learning for the first time.

Vision-Conditioned Control. Much work has been done on end-to-end driving, directly learning a mapping from pixels to control signals [35]. Numerous reinforcement learning approaches have been proposed for racing [36], [37], focusing on learning an NN policy. Also in MPC, vision-conditioning has been applied to infer cost [38], [39] or derive constraints for obstacle avoidance [38], but not to condition a dynamics model. Although recent methods learn MPC dynamics within an RL framework for aggressive driving, they do not incorporate vision [40]. In mobile robotics, visual foundation models have been used to estimate disturbances for a nominal physics-based dynamics model [41], and perceptive dynamics models have been proposed for legged robots using exteroceptive inputs to enable safe planning [42] with MPPI. To our knowledge, our approach is the first to explicitly condition a dynamics model on vision with downstream use in an optimal controller for proactive racing. Our results show that this capability can be the difference-maker when racing autonomously in varying friction conditions.

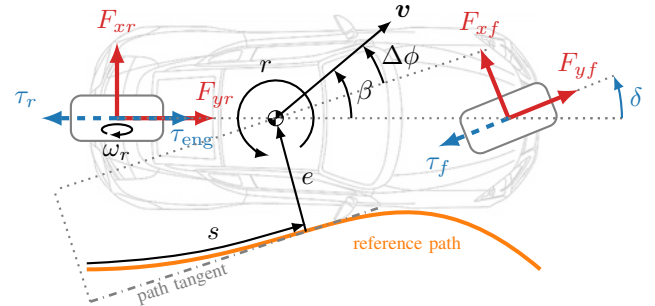


Fig. 2. Vehicle geometry with the bicycle model states \mathbf{x} (black), control inputs \mathbf{u} (blue), tire forces (red), and the reference path $\mathbf{x}_{\text{ref}}(s)$ (orange).

III. PRELIMINARIES

Vectors are denoted by $\mathbf{x} \in \mathbb{R}^n$, with x_i being the i th element of \mathbf{x} . Matrices are indicated in bold, \mathbf{X} , and the element on row i and column j of \mathbf{X} is $[\mathbf{X}]_{ij}$. We let

$$\mathbf{x} \sim \mathcal{N}(\mathbf{x}|\mathbf{m}, \mathbf{P}) \propto |\mathbf{P}|^{-1/2} \exp(-\frac{1}{2}(\mathbf{x}-\mathbf{m})^\top \mathbf{P}^{-1}(\mathbf{x}-\mathbf{m}))$$

indicate that the random variable \mathbf{x} is Gaussian distributed with mean \mathbf{m} and covariance \mathbf{P} . Similarly, we let

$$\underline{x} \sim \text{IG}(x|\alpha, \beta) \propto x^{-\alpha-1} \exp(-\beta x^{-1}),$$

indicate that \underline{x} is inverse Gamma distributed. We write the expectation of $\mathbf{x} \sim p_{\underline{x}}(\mathbf{x})$ as $\mathbb{E}_{\mathbf{x} \sim p_{\underline{x}}(\mathbf{x})}[\mathbf{x}] = \int \mathbf{x} p_{\underline{x}}(\mathbf{x}) d\mathbf{x}$ compactly as $\mathbb{E}_{\underline{x}}[\mathbf{x}]$. In this notation, the KL-divergence between the densities p and q is $\text{KL}(p\|q) = \mathbb{E}_p[\log(p(\mathbf{x})/q(\mathbf{x}))]$.

Physics-based models. In [3], [14], [31], it is shown that a well-calibrated single-track model [19] with Fiala tire-forces [4], [20] enables racing at the limits of handling (see Fig. 2). Thus, we use similar inputs for our learned model, and define the state $\mathbf{x} = (\mathbf{x}_1, \mathbf{x}_2)$ and control input \mathbf{u} as

$$\mathbf{x}_1 = (r, v, \beta, \omega_r)^\top \in \mathbb{R}^4, \quad (1a)$$

$$\mathbf{x}_2 = (e, \Delta\phi, s)^\top \in \mathbb{R}^3, \quad (1b)$$

$$\mathbf{u} = (\delta, \tau_{\text{combined}}, \tau_f)^\top \in \mathbb{R}^3, \quad (1c)$$

where r (rad/s) is a yaw rate, v (m/s) is the longitudinal velocity, β (rad) is a side-slip angle, and ω_r (rad/s) is an average rear wheel speed, e (m) is a lateral path distance, $\Delta\phi$ (rad) is a deviation with respect to a racing line, and s (m) is a path distance (see Fig. 2). Furthermore, δ (rad) is the steering angle, τ_{combined} (Nm) is the combined rear torque, and τ_f (Nm) are the front brake torques. The dynamics of the vehicle can then be written as a cascaded system

$$\dot{\mathbf{x}}_1(t) = \mathbf{f}_1(\mathbf{x}_1(t), \mathbf{u}(t)), \quad (2a)$$

$$\dot{\mathbf{x}}_2(t) = \mathbf{f}_2(\mathbf{x}_1(t), \mathbf{x}_2(t), \mathbf{u}(t)). \quad (2b)$$

In this representation, \mathbf{f}_1 encodes assumptions about the tire-force model and is defined by parameters that are estimated or manually tuned (see the appendix), whereas \mathbf{f}_2 is known

from the car's kinematics. Indeed, from Fig. 2, we obtain

$$\dot{e}(t) = v(t) \sin(\Delta\phi(t)), \quad (3a)$$

$$\Delta\dot{\phi} = \dot{\beta}(t) + r(t) - \frac{\kappa_{\text{ref}}(t)v(t) \cos(\Delta\phi(t))}{(1 - \kappa_{\text{ref}}(t)e(t))}, \quad (3b)$$

$$\dot{s}(t) = \frac{v(t) \cos(\Delta\phi)}{(1 - \kappa_{\text{ref}}(t)e(t))}, \quad (3c)$$

where κ_{ref} is the signed curvature of the reference path. The term \mathbf{f}_1 contains all the epistemic uncertainty of the vehicle model, and is the focus of our learning based methods. To embed this model in a predictive control framework, we reparametrize the model in the path variable s , as

$$\frac{d}{ds}\mathbf{x}(s) = \frac{1}{\dot{s}} \begin{bmatrix} \mathbf{f}_1(\mathbf{x}_1(s), \mathbf{u}(s)) \\ \dot{e}(s) \\ \Delta\dot{\phi}(s) \\ 1 \end{bmatrix} \triangleq \mathbf{f}(\mathbf{x}(s), \mathbf{u}(s)). \quad (4a)$$

We then discretize the dynamics with a constant path step $\Delta s = 3 \text{ m}$ and integrate the ODE with explicit Euler as

$$\mathbf{x}_{k+1} = \mathbf{x}_k + \Delta s \mathbf{f}(\mathbf{x}_k, \mathbf{u}_k). \quad (5)$$

Optimal Control. In the context of racing, the objective is to minimize lap time. Following [3], we penalize state-control deviations from a pre-computed reference trajectory $(\mathbf{x}_{\text{ref}}(s), \mathbf{u}_{\text{ref}}, \kappa_{\text{ref}}(s))_{s>0}$ and rapid changes in control inputs to improve robustness and numerical stability. We define the linear time cost and quadratic stage costs as:

$$\ell_T(\mathbf{x}) = \lambda_T t, \quad (6a)$$

$$\ell(\mathbf{x}, \mathbf{u}, \mathbf{u}_-) = \|\mathbf{x} - \mathbf{x}_{\text{ref}}\|_Q^2 + \|\mathbf{u} - \mathbf{u}_{\text{ref}}\|_R^2 + \frac{\|\mathbf{u} - \mathbf{u}_-\|_T^2}{(\Delta s)^2}, \quad (6b)$$

where $\|\mathbf{v}\|_P^2 = \mathbf{v}^\top \mathbf{P} \mathbf{v}$, and $(\mathbf{Q}, \mathbf{R}, \mathbf{T})$ are diagonal weight matrices with small entries compared to terminal time cost ℓ_T (see the appendix). The term $\|\mathbf{u} - \mathbf{u}_-\|_T^2/(\Delta s)^2$ penalizes control rates, where \mathbf{u}_- is the previous control input. With these costs, we formulate the optimal control problem (OCP):

$$\min_{\mathbf{x}_{0:N}} \ell_T(\mathbf{x}_N) + \sum_{k=0}^{N-1} \ell(\mathbf{x}_k, \mathbf{u}_k, \mathbf{u}_{k-1}) \quad (7)$$

$$\begin{aligned} \text{s.t. } & \mathbf{F}(\mathbf{x}_k, \mathbf{u}_k, \mathbf{x}_{k+1} \mid \mathbf{c}_t) = \mathbf{0}, & k \in [0, N-1] \\ & (\mathbf{x}_0, \mathbf{u}_0) = (\mathbf{x}_{\text{init}}, \mathbf{u}_{\text{init}}), \\ & \mathbf{u}_{\text{min}} \leq \mathbf{u}_k \leq \mathbf{u}_{\text{max}}, & k \in [0, N-1] \\ & e_{\text{min},k} \leq e_k \leq e_{\text{max},k}, & k \in [0, N] \end{aligned}$$

where \mathbf{F} represents the combined dynamics given the current context \mathbf{c}_t , enforcing (5). This formulation results in a context-dependent optimal control problem that is solved in a receding horizon fashion. The car is actuated with the optimal controls $\mathbf{u}_{0:N-1}^*$ linearly interpolated to the current position of the car in s . Next, we describe how to express \mathbf{F} using VBLLs.

IV. VBLLS WITH FiLM CONDITIONING

We begin in Sec. IV-A by describing how to learn a base VBLL dynamics model from state transitions only. Sec. IV-B explains how to extract visual context from limited data, and Sec. IV-C details how to condition the VBLL model on this context in a fine-tuning step with limited data (see Fig. 3).

A. Learning a VBLL vehicle model

Following common practice in dynamics learning [8], [43], we train a VBLL model to predict state differences rather than absolute states, which has been shown to improve numerical stability [8]. We learn the dynamics (2a) in time coordinates and then convert to path coordinates using (4a). Specifically, for a time step $\Delta t > 0$, we model

$$\Delta\mathbf{x}_t := \mathbf{x}_{1,t+\Delta t} - \mathbf{x}_{1,t} = \mathbf{f}_\theta(\mathbf{z}_t), \quad (8)$$

where \mathbf{f}_θ denotes the learned dynamics function parameterized by θ , and $\mathbf{z}_t = [\mathbf{x}_{1,t}, \mathbf{u}_t, \mathbf{u}_{t+\Delta t}] \in \mathbb{R}^{n_z}$ contains the relevant states and controls at time t along with the controls at the next time step.¹ Selecting a Δt to approximately match the discrete path step Δs at the expected average velocity will later allow us to directly integrate the learned model using the discretization scheme in (5).

Remark 1: As in [2], [3], we include the control input at the next time step in the dynamics model inputs, consistent with our MPC implementation that interpolates the control sequence in s at runtime.

Given the training target description in (8), we now define the VBLL model architecture that learns to predict these state differences in a supervised manner. We define a VBLL model with d independent heads as

$$\mathbf{f}_\theta(\mathbf{z}_k) = \varphi_\theta(\mathbf{z}_k)^\top \mathbf{W} = \varphi_\theta(\mathbf{z}_k)^\top [\mathbf{w}_1, \dots, \mathbf{w}_d], \quad (9)$$

where $\varphi_\theta : \mathbb{R}^{n_z} \mapsto \mathbb{R}^{n_w}$ are learned features and $\mathbf{w}_i \in \mathbb{R}^{n_w}$ are Gaussian random variables associated with each VBLL prediction head. Sampling the state difference (8) in practice is noisy, and we therefore define a measurement model

$$\mathbf{y}_k = \mathbf{f}_\theta(\mathbf{z}_k) + \boldsymbol{\varepsilon}_k, \quad (10)$$

where $\boldsymbol{\varepsilon}_k$ is independent Gaussian zero-mean noise with covariance $\Sigma = \text{diag}(\Sigma_1, \dots, \Sigma_d)$. To infer the backbone parameters, weight distribution, and noise statistics, we follow [44] and assume a zero-mean Gaussian prior with covariance $p(\mathbf{w}_i) = \mathcal{N}(\mathbf{w}_i; \mathbf{0}, \xi_i^\circ \mathbf{I})$ for the i th head. The measurements in (10) are Gaussian given (9). As the Gaussian is its own conjugate prior, we define the posterior

$$q(\mathbf{W}) = \prod_{i=1}^d q(\mathbf{w}_i) = \prod_{i=1}^d \mathcal{N}(\mathbf{w}_i; \mathbf{m}_i, \mathbf{S}_i), \quad (11)$$

and let $\mathbf{S}_i = \mathbf{L}_i \mathbf{L}_i^\top$ where $\mathbf{L}_i = \mathbf{N}_i + \text{diag}(\exp(\mathbf{d}_i))$ is lower-triangular and $\text{diag}(\mathbf{N}_i) = \mathbf{0}$. This ensures that \mathbf{S}_i is positive definite without imposing explicit constraints during training. For ease of notation, we define the learnable parameters of the VBLL heads as $\eta = \{\mathbf{m}_i, \mathbf{N}_i, \mathbf{d}_i, \Sigma_i\}_{i=1}^d$.

Remark 2: This approach differs from the BLL in [2] in that η includes the unknown noise statistics $\{\Sigma_i\}_{i=1}^d$, giving the model more flexibility. As in [2], our model allows for online adaptation, which is one of our baselines in Sec. V.

Losses. Let $\mathcal{D} = \{(\mathbf{z}_j, \mathbf{y}_j)\}_{j=1}^{|\mathcal{D}|}$ denote our training dataset, where each sample consists of inputs \mathbf{z}_j and the corresponding

¹The subscript t is a time (continuous) and k is a path coordinate (discrete).

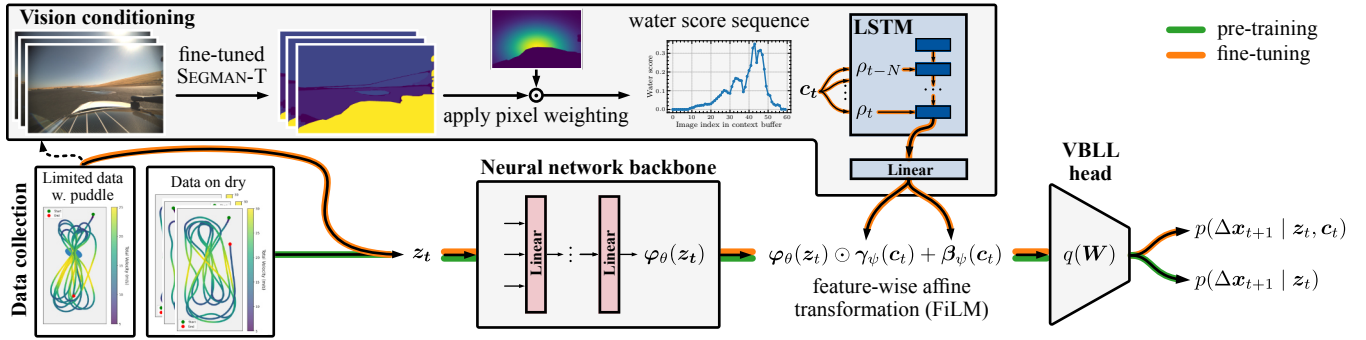


Fig. 3. *Conceptual overview of VcVBLL and its training.* We begin by training a base VBLL dynamics model (green path). To incorporate vision-based conditioning, we first extract semantic classes using a fine-tuned SEGMAN-T backbone from the limited available data with water interaction, from which we compute a short 2 sec time series of past water scores corresponding to c_t . In a subsequent fine-tuning phase, this time series is encoded with an LSTM and used in a FiLM conditioning path to obtain our vision-conditioned VcVBLL dynamics model (orange path).

measured state differences \mathbf{y}_j . We standardize all inputs and outputs to have a zero mean and unit variance, thereby improving training stability and convergence. We seek to maximize the evidence lower bound (ELBO) derived in [44, Theorem 1]. Given the weights in (11) the noise in (10) are both independent across the VBLL heads, we get

$$\mathcal{L}_{\text{ELL}}(\eta, \theta) = \frac{1}{|\mathcal{D}|} \sum_{j=1}^{|\mathcal{D}|} \sum_{i=1}^d \left[\log N(y_{ji} | \varphi_\theta(z_j)^\top \mathbf{m}_i, \Sigma_i) - \frac{1}{2} \varphi_\theta(z_j)^\top S_i \varphi_\theta(z_j) \Sigma_i^{-1} \right], \quad (12)$$

as a lower bound on the expected log-likelihood (ELL) of \mathcal{D} . Following [44], we also introduce a regularizer

$$\mathcal{R}(\eta, \theta) = \frac{1}{|\mathcal{D}|} \sum_{i=1}^d \left[-\text{KL}(q(\mathbf{w}_i) || p(\mathbf{w}_i)) - \log N(\theta | \mathbf{0}, \gamma^\circ \mathbf{I}) - \log \text{IG}(\Sigma_i | \alpha_i^\circ, \beta_i^\circ) \right]. \quad (13)$$

weighted by $\lambda_{\text{reg}} > 0$ to stabilize training and regularize the densities toward suitable priors defined by $\{\alpha_i^\circ, \beta_i^\circ, \gamma^\circ, \xi_i^\circ\}_{i=1}^d$. Combining both parts, we formulate and solve the following optimization problem

$$\bar{\theta}, \bar{\eta} = \arg \min_{\theta, \eta} \underbrace{[-\mathcal{L}_{\text{ELL}}(\eta, \theta) + \lambda_{\text{reg}} \mathcal{R}(\eta, \theta)]}_{:= \mathcal{L}(\eta, \theta)}, \quad (14)$$

with additional details on the priors, specifications of the MLP backbone φ , and considered regularizers given in the Appendix. With the learned parameters, we obtain a posterior predictive given an input at time t as

$$y_{ti} | \mathbf{z}_t \sim N(\varphi_{\bar{\theta}}(\mathbf{z}_t)^\top \bar{\mathbf{m}}_i, \varphi_{\bar{\theta}}(\mathbf{z}_t)^\top \bar{S}_i \varphi_{\bar{\theta}}(\mathbf{z}_t) + \bar{\Sigma}_i). \quad (15)$$

To use this model in the intended racing application, we use the maximum a posteriori (MAP) estimate of the learned state difference in the ODE (2a) of the states \mathbf{x}_1 , and let

$$\dot{\mathbf{x}}_1(t) \approx \varphi_{\bar{\theta}}(\mathbf{z}_t)^\top [\bar{\mathbf{m}}_1, \dots, \bar{\mathbf{m}}_d] / \Delta t. \quad (16)$$

This approach allows us to use the curvilinear coordinates and reparametrize the dynamics in path distance (4a), discretize the dynamics in s (5), and formulate the OCP (7) in Sec. III.

B. Extracting Contextual Visual Information

Backbones. To extract meaningful visual context for the learned model in Sec. IV-A, we use SEGMAN [45] to segment images captured on the car. We also evaluated SEGNEXT [46] and SEGFORMER [47], but found SEGMAN superior in both speed and accuracy for our driving application. We use the tiny model and train it from scratch on the public GOOSE dataset [48], which contains 10k images of rural and off-road driving in Germany. This setting better matches racing conditions, which are closer to rural than urban environments, yielding better embeddings. To further improve performance, we fine-tune the model on 500 manually labeled images from the California test location used in our experiments. We retain the 64 closed-set classes of the GOOSE dataset, represented by unique integers $\mathcal{C} = \{1, \dots, 64\}$. At inference, this yields a segmented image $\hat{I}_k \in [|\mathcal{C}|]^{W \times H}$ of size $(W, H) = (1440, 928)$. Example outputs are shown in Fig. 3.

Weighting. To extract semantically meaningful surface information from this output, we compute a spatially weighted water presence score. This score emphasizes the region of the image most relevant to the vehicle’s trajectory. We define a Gaussian weighting mask over the image domain. At pixel coordinates $(w, h) \in [W] \times [H]$, the weight is given by

$$w(h, w) = \exp \left(- \left[\frac{(h - \mu_h)^2}{2\sigma_h^2} + \frac{(w - \mu_w)^2}{2\sigma_w^2} \right] \right), \quad (17)$$

where $\mu_h \in [H]$ and $\mu_w \in [W]$ and $\sigma_h, \sigma_w > 0$ control its spread in the vertical and horizontal directions, respectively. This approach focuses attention on a region of interest, such as the road area directly ahead of the vehicle, and down-weights potential outliers on the edge of the image (see Fig. 3).

Context. Without loss of generality, we consider two classes:

- $c_w \in \mathcal{C}$: the class label corresponding to water;
- $c_a \in \mathcal{C}$: the class label corresponding to asphalt.

Furthermore, let $\Omega \subset [W] \times [H]$ denote the set of pixels that are not occluded (i.e., not part of the vehicle body), for which the weight is non-zero. We then define a “water score” as

$$\rho_t = \frac{\sum_{(w,h) \in \Omega} w(h, w) \cdot \mathbf{1}\{\hat{I}_k = c_w\}}{\sum_{(w,h) \in \Omega} w(h, w) \cdot [\mathbf{1}\{\hat{I}_k = c_w\} + \mathbf{1}\{\hat{I}_k = c_a\}]}, \quad (18)$$

where $\mathbf{1}\{\cdot\}$ denotes the indicator function. This ratio provides a normalized measure of the prevalence of water relative to asphalt in the spatial region emphasized by the Gaussian. In general, if there are more classes of relevance, such as ice or gravel, we can easily extend (18) to a vector-valued score, with the relative prevalence of each class of interest. In the following, we provide the context $\mathbf{c}_t = (\rho_{t-N}, \dots, \rho_t)$ of the current surface condition to the learned dynamics models.

C. Vision-based Conditioning using FiLM

To incorporate contextual visual information into our learned dynamics model, we employ Feature-wise Linear Modulation (FiLM) [25]. This approach allows the visual context to adaptively modulate the backbone network's features through learned affine transformations. FiLM relies on a conditioning function $g_\psi(\cdot)$ that maps the contextual input to modulation parameters. We implement this function as a Long Short-Term Memory (LSTM) network [49], with

$$(\gamma_\psi(\mathbf{c}_t), \beta_\psi(\mathbf{c}_t)) = g_\psi(\mathbf{c}_t), \quad (19)$$

where g_ψ is parameterized by LSTM weights ψ , and the factors $\gamma(\mathbf{c}_t)$ and shift parameters $\beta(\mathbf{c}_t)$ have the same dimensionality as the backbone features (see Sec. IV-B). While it is possible to use simple MLPs, the LSTM is chosen to better capture temporal dependencies in the context \mathbf{c}_t .

Modulation. The backbone features of the VBLL are modulated as in [25], with an element-wise affine transformation

$$\tilde{\varphi}_t := \varphi_{\{\theta, \psi\}}^{\text{FiLM}}(\mathbf{z}_t, \mathbf{c}_t) = \varphi_\theta(\mathbf{z}_t) \odot \gamma_\psi(\mathbf{c}_t) + \beta_\psi(\mathbf{c}_t), \quad (20)$$

where \odot denotes element-wise multiplication. This formulation enables the visual context to selectively amplify or suppress different feature dimensions based on the observed surface conditions, allowing the model to adapt its internal representations to account for varying road surface properties. Finally, we formulate the conditional posterior predictive

$$\Delta \mathbf{x}_{t+1,i} \mid \mathbf{z}_t, \mathbf{c}_t \sim \mathcal{N}(\tilde{\varphi}_t^\top \mathbf{m}_i, \tilde{\varphi}_t^\top \mathbf{S}_i \tilde{\varphi}_t + \Sigma_i). \quad (21)$$

D. Data Collection, Training, and Fine-Tuning

Data Collection. An expert driver operated a Lexus LC500 on a skidpad under controlled conditions to collect training data. The nominal dataset, containing $|\mathcal{D}| = 12\,229$ samples for training, was obtained through a series of aggressive maneuvers designed to excite the full range of the nonlinear vehicle dynamics in nominal, i.e., dry, conditions (see Fig. 3).

For the fine-tuning dataset, we introduced a water puddle on the skidpad. The driver then repeated similar aggressive maneuvers to capture transient tire-surface interactions under wet conditions (cf. Fig. 3, bottom left). High ambient temperatures and sun exposure at the test site caused rapid evaporation, making this data collection process slow and labor-intensive, which highlights the utility of our fine-tuning approach. The fine-tuning dataset comprises 6349 samples, of which only 1540 (approx. 24%) contain a non-zero context vector \mathbf{c}_t . Since \mathbf{c}_t spans a two-second window, the direct exposure to wet conditions is even more limited.

Training Procedure. We first train the base VBLL dynamics model on the nominal dataset by minimizing the loss in (14). To enhance numerical stability, all input and output features are standardized prior to training. The same standardization parameters are applied to the fine-tuning dataset to ensure feature consistency. We then use this trained base VBLL model as the initialization for the subsequent fine-tuning to learn the conditional path (i.e., the orange path in Fig. 3).

To prevent catastrophic forgetting, we augment the base loss from (14) with an L2-SP regularization term [50], and solve the following optimization problem using the fine-tuning dataset

$$\bar{\theta}, \bar{\eta}, \bar{\psi} = \arg \min_{\theta, \eta, \psi} \left[\mathcal{L}(\eta, \{\theta, \psi\}) + \lambda_{\text{L2-SP}} \|\theta - \theta_{\text{init}}\|_2^2 \right], \quad (22)$$

where θ_{init} are the parameters of the VBLL model trained with a loss (14) using only dry data (green path in Fig. 3). We refer to the resulting finetuned model as VcVBLL.

V. RESULTS

We test the proposed VcVBLL vehicle model in closed-loop MPC on a Lexus LC500. We discuss the effect of the visual context in Sec. V-A and then present hardware results with baseline models, with and without the vision context, when racing through puddles in Sec. V-B. A video of the experiments is available at: <https://youtu.be/m-gcFK0moI8>.

A. Intuition on the Effect of Vision Conditioning

To illustrate the effect of the vision context on model predictions, we study the fine-tuned VcVBLL described in Sec. IV-C, with and without vision context. We use segmentation outputs recorded in the car while racing through a puddle, and show the posterior predictive (21) as a function of the steering input δ at different points in time (see Fig. 4).

The VcVBLL predictions diverge upon detecting water ($t = 15$): with the context, the wheels are predicted to slip and spin more, and the car is also predicted to lose traction and gain more sideslip under the same actuation. Notably, the difference induced by the context is maximal after a small delay, corresponding to the time between detecting water and the vehicle entering the puddle ($t = 20$). These differences in prediction persist for some time due to the tires remaining wet after having passed through the puddle ($t = 25$). Over time, the impact of water on the dynamics becomes negligible ($t = 30$). The effect of the vision context on the VBLL predictions thus makes sense physically. The presence of water also inflates the uncertainty of the predictive posterior, which is expected as the vehicle dynamics become harder to model accurately under such transient surface conditions.

B. Hardware Experiments

Setup. We validate the proposed method on the LC500 vehicle depicted in Fig. 1. The segmentation backbone is run on an L4 GPU, and all other computations are done on a 3.30GHz Intel Xeon E-2278GE CPU. This includes evaluating the FiLM modulation and solving the OCP via sequential quadratic programming [51, Chapter 18] using the

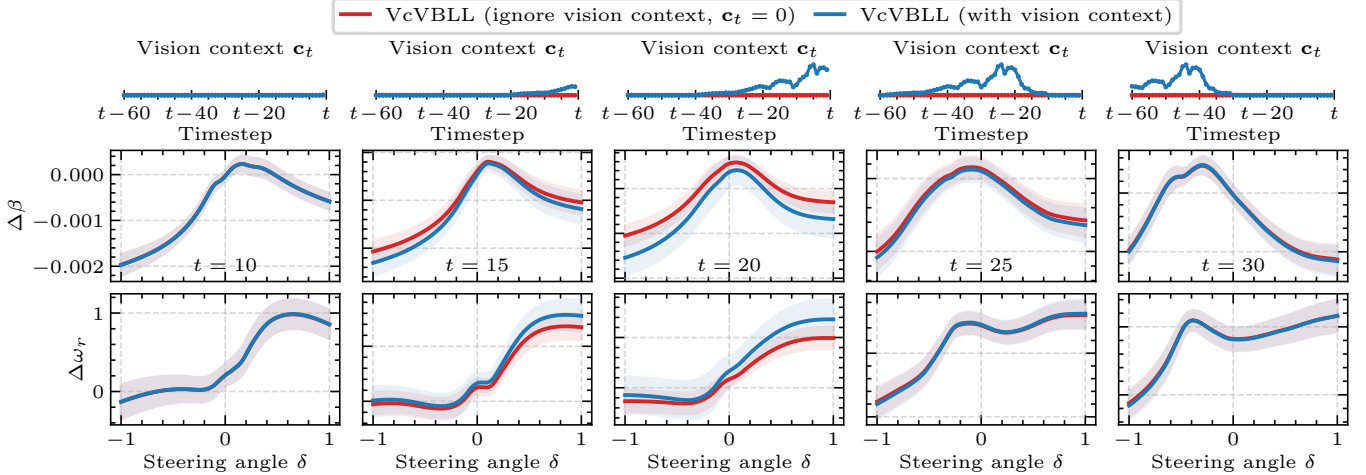


Fig. 4. *Slices through the VcVBLL posterior when driving over a puddle.* After fine-tuning, the VcVBLL model can effectively provide conditional prediction based on the provided visual context, as seen by the difference in posterior predictive distributions for the selected states. Moreover, the model’s behavior is physically plausible: a wet surface results in higher wheel speeds and increased side-slip dynamics, as well as increased uncertainty.

TABLE I

LAP TIME OF BASELINE METHODS FOR FIGURE 5 WITHOUT PUDDLE.

	Physics-based	VBLL	VcVBLL
Lap time	24.53 sec	24.06 sec	24.24 sec

OSQP solver [52]. The vehicle states are estimated using an OxTS system [53], and the images are sampled from a single forward-facing Lucid Ti 3.2MP camera [54] (see Fig. 3). With this setup, the segmentation runs at approximately 25–30Hz, and is therefore separated in a different thread to not prevent the execution of the controller. Compared to the offline training data for the FiLM conditioning, which provides segmentation results at 30Hz, some frames are dropped in the experiments. Consequently, we align the vehicle states with the images and populate the missing frames by interpolating the water score. When present, the modulating FiLM signal is computed at 7Hz, while the controller is running at 62.5Hz.

Racing Baselines. To verify that the learned VBLL serves as a suitable evaluation baseline, we first test it in hardware using the deterministic minimum-time MPC formulation from [3] (without puddles), and compare:

- The physics-based vehicle model used in [3];
- A baseline VBLL vehicle model, similar to that of [2];
- A VcVBLL model derived from the baseline VBLL.

We consider the racing task in [3], and report results in Fig. 5. We observe that the controllers using the OCPs formulated with VBLL models better utilize the available rear tire force by applying more throttle, resulting in more rear wheel speed (see ω_r), sideslip (see β), and ultimately velocity (see v) when exiting the corner. Performance is reduced marginally in VcVBLL compared to VBLL, but both methods still beat the physics-based model in lap times (see Tab. I). Next, we introduce water on the track and study the effect of vision.

Racing Through Puddles. To study how the vision context affects closed-loop control, we place a large puddle near the exit of the first turn and replenish it with equal amounts of water between each consecutive experiment. We use the

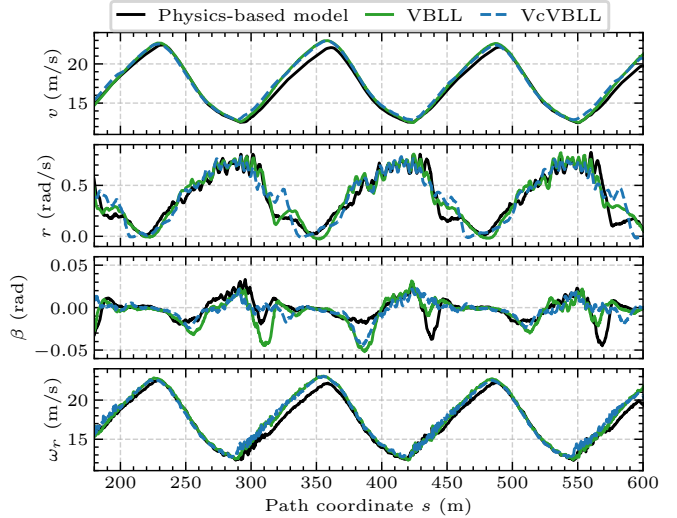


Fig. 5. *Performance of VBLL dynamics model on the dry track.* With a learned dynamics model (VBLL and VcVBLL) the MPC is able to achieve higher velocities resulting in faster lap times (cf. Table I).

minimum-time MPC with dynamics constraints from:

- The baseline VBLL vehicle model;
- The VBLL model with RLS adaptation, as in [2];
- The VcVBLL model ignoring vision context;
- The VcVBLL model utilizing vision context.

The results from one of three sets of experiments are shown in Fig. 6, and indicate that the vision context is crucial for the car to drive safely through the puddle. In particular, as soon as there is a signal from the segmentation that water will be present, the controller preemptively drops the engine torque and engages the brakes, which reduces the side-slip on exit and allows the vehicle to recover and continue racing. The VcVBLL without vision context exhibits similar behavior in engine torque, but does not initiate the brakes and spins out as a result. These experiments were repeated three times, with the VcVBLL using vision context completing all 9 laps through the water successfully. We conclude that the vision context, albeit simplistic, allows for preemptive control through the MPC, and is the unambiguous difference maker between

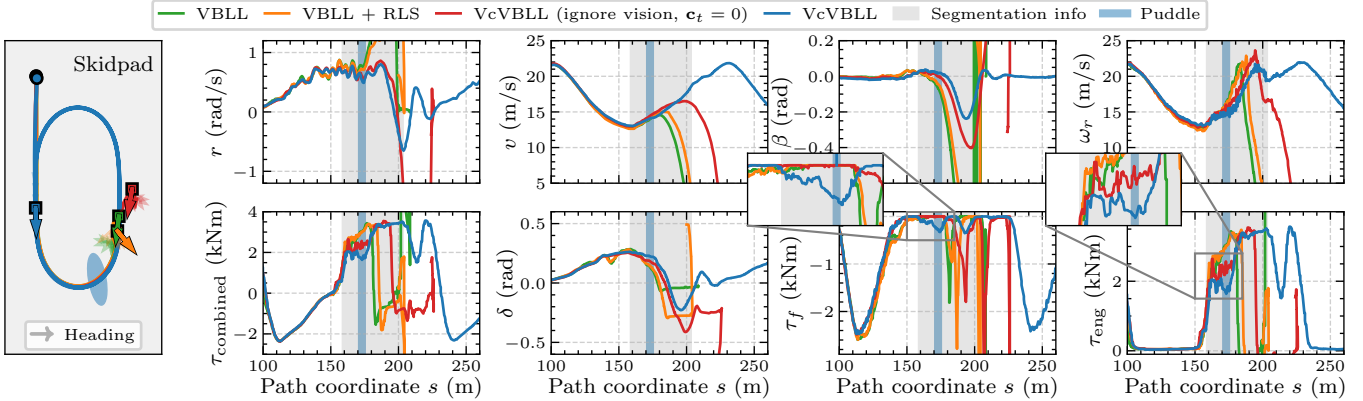


Fig. 6. Hardware experiments comparing various methods in a racing task with water placed on the exit of a turn. All methods spin out after driving through the puddle, except for the VcVBLL with vision context, which completes three laps before the experiment is stopped manually.



Fig. 7. Difference in lighting conditions in the August and September tests.

TABLE II

PERCENTAGE OF SUCCESSFUL ATTEMPTED TURNS THROUGH A PUDDLE.

Occasion	VBLL	VBLL + RLS	VcVBLL ($c_t = 0$)	VcVBLL
August	0 (0/1)	0 (0/1)	—	100 (3/3)
September	0 (0/3)	0 (0/1)	0 (0/1)	100 (9/9)

staying on track and spinning out.

Robustness. To test robustness to vehicle parameter changes like road conditions and tire wear, we deployed the method twice with (i) different tires, (ii) 15°C temperature difference, and (iii) different lighting (see Fig. 7). We slightly re-tuned the parameters of the controller for all baselines, using $\lambda_T = 500$ on the first occasion and $\lambda_T = 200$ on the second occasion.

The hardware results were repeatable, as shown in Tab. II, with one set of experiments from the second row illustrated in Fig. 6. In total, across the two test sessions, the baselines spun out every single time (although the baseline VcVBLL ignoring vision was not tested in August). In contrast, the VcVBLL with vision context completed 12 out of 12 attempted laps, indicating that it is robust to experimental conditions.

VI. CONCLUSION

This letter presents a vision-conditioned VBLL vehicle model that enables proactive control in autonomous racing under varying surface conditions. By conditioning the dynamics model on visual context via FiLM, a controller can anticipate changes in road surface properties before encountering them. Our approach employs a two-stage training strategy: first learning a nominal VBLL model on dry surface data, then fine-tuning the conditioning path using the limited available data of water interactions. Hardware experiments on a Lexus LC500 racing through water puddles demonstrate the efficacy of the approach: the vision-conditioned model

completed multiple laps across varying conditions, while baseline methods without visual context consistently spun out. These results demonstrate that incorporating exteroceptive information into learned dynamics models is essential for safe and robust autonomous racing in changing conditions. Future work will explore the use of vision-conditioned models for predictive control in other applications, such as autonomous drifting and off-road driving with a richer visual context.

APPENDIX

Physics-based vehicle model The dynamics in (2a) are

$$\dot{r} = (aF_{yf} \cos(\delta) + aF_{xf} \sin(\delta) - bF_{yr})/I_z, \quad (23a)$$

$$\dot{v} = (-F_{yf} \sin(\delta - \beta) + F_{xf} \cos(\delta - \beta) + F_{yr} \sin \beta + F_{xr} \cos \beta)/m, \quad (23b)$$

$$\dot{\beta} = -r + (F_{yf} \cos(\delta - \beta) + F_{xf} \sin(\delta - \beta) + F_{yr} \cos \beta - F_{xr} \sin \beta)/(mv), \quad (23c)$$

$$\dot{\omega}_r = (\tau_{eng} - F_{xr} r_w)/I_w, \quad (23d)$$

with parameters $(a, b, I_z, m, r_w, I_w) \in \mathbb{R}_{>0}^6$. The tire forces $F_{xf}, F_{yf}, F_{xr}, F_{yr}$ (N) are nonlinear functions of the state (see, e.g. [3] for details) parametrized in cornering stiffness $(C_f, C_r) \in \mathbb{R}_{>0}^2$ and friction coefficients $(\mu_f, \mu_r) \in \mathbb{R}_{>0}^2$, with f and r referring to the front and rear wheels, respectively. The parameters are found by physical measurements and gray-box system identification. The parameters used in the experiments are summarized in SI units in Tab. III.

TABLE III
MODEL PARAM.

Param.	Value
a	1.3457754
b	1.5222246
I_z	3675
m	2048
r_w	0.368
I_w	30
C_f	156000
C_r	422000
μ_f	1.02
μ_r	1.08

Baseline VBLL Model and Training Details. For the backbone of the VBLL model, we use 4 hidden layers with 64 neurons and ELU activations. The LSTM of the FiLM VBLL has a latent state size of 16 and we use an additional linear layer to decode this latent to the FiLM vectors (cf. Fig. 3). For the VBLL heads, we set $\xi_i^\circ = 1$, $\alpha_i^\circ = \frac{1}{2}$, and $\beta_i^\circ = \frac{0.01}{2}$. We implicitly set γ° by adding weight decay of 10^{-4} on the backbone as in [33] and using AdamW [55] with a learning rate of $5 \cdot 10^{-4}$ for the base model and 10^{-4} for fine-tuning. We further use a gradient clipping of 1 for both. For the base

model, we train for 5000 epochs and for the fine-tuning for 1000, but use the best performing model based on a holdout validation set. For both, we use a batch size of 1028. The regularization parameters are $\lambda_{\text{reg}} = 10$ and $\lambda_{\text{L2-SP}} = 10$.

Controller parameters. The nominal MPC weights are $\lambda_T = 500$, $Q = \text{diag}(10, 0.1, 1, 10^{-8}, 0.01, 10, 0.01, 0)$, $R = \text{diag}(0.1, 10^{-4}, 10^{-5})$, $T = \text{diag}(2 \cdot 10^5, 10^{-5}, 10^{-9})$.

ACKNOWLEDGMENT

The authors acknowledge Steven Goldine for driving in the data collection, Emre Adabag for helpful discussions, and William Kettle, Phung Nguyen, Zachary Conybeare, and Max Freeman for support in the experiments.

REFERENCES

- [1] J. Dallas, M. Thompson, J. Y. Goh, and A. Balachandran, “Adaptive nonlinear model predictive control: maximizing tire force and obstacle avoidance in autonomous vehicles,” *Field Robotics*, 2023.
- [2] A. Davydov, F. Djeumou, M. Greiff, M. Suminaka, M. Thompson, J. Subosits, and T. Lew, “First, learn what you don’t know: Active information gathering for driving at the limits of handling,” *IEEE Robotics and Automation Letters*, 2025.
- [3] T. Lew, M. Greiff, F. Djeumou, M. Suminaka, M. Thompson, and J. Subosits, “Risk-averse model predictive control for racing in adverse conditions,” in *Int. Conf. on Robotics and Automation*, 2025.
- [4] J. Svendenius, “Tire modeling and friction estimation,” Ph.D. dissertation, Lund University, 2007.
- [5] C. R. Carlson and J. C. Gerdes, “Nonlinear estimation of longitudinal tire slip under several driving conditions,” in *American Control Conference*. IEEE, 2003.
- [6] K. Berntorp, “Particle filtering and optimal control for vehicles and robots,” Ph.D. dissertation, Lund University, 2014.
- [7] F. Djeumou, T. J. Lew, N. Ding, M. Thompson, M. Suminaka, M. Greiff, and J. Subosits, “One model to drift them all: Physics-informed conditional diffusion model for driving at the limits,” in *Conference on Robot Learning*, 2024.
- [8] N. Ding, M. Thompson, J. Dallas, J. Y. Goh, and J. Subosits, “Drifting with unknown tires: Learning vehicle models online with neural networks and model predictive control,” in *Int. Vehicles Sym.*, 2024.
- [9] M. Suminaka, J. Dallas, M. Thompson, M. Soga, E. Kasai, and J. Subosits, “Adaptable high-speed model predictive control for autonomous drifting,” in *ACC*. IEEE, 2025.
- [10] J. Kabzan, L. Hewing, A. Liniger, and M. N. Zeilinger, “Learning-based model predictive control for autonomous racing,” *IEEE Robotics and Automation Letters*, 2019.
- [11] L. Hewing, J. Kabzan, and M. N. Zeilinger, “Cautious model predictive control using gaussian process regression,” *IEEE Trans. on Control Systems Technology*, 2019.
- [12] F. Djeumou, J. Y. Goh, U. Topcu, and A. Balachandran, “Autonomous drifting with 3 minutes of data via learned tire models,” *ICRA*, 2023.
- [13] G. Williams, P. Drews, B. Goldfain, J. M. Rehg, and E. A. Theodorou, “Aggressive driving with model predictive path integral control,” in *IEEE International Conference on Robotics and Automation*, 2016.
- [14] N. A. Spielberg, M. Brown, and J. C. Gerdes, “Neural network model predictive motion control applied to automated driving with unknown friction,” *IEEE Trans. on Control Systems Technology*, 2021.
- [15] J. K. Subosits and J. C. Gerdes, “Impacts of model fidelity on trajectory optimization for autonomous vehicles in extreme maneuvers,” *IEEE Trans. on Intelligent Vehicles*, 2021.
- [16] J. Dallas, M. P. Cole, P. Jayakumar, and T. Ersal, “Terrain adaptive trajectory planning and tracking on deformable terrains,” *IEEE Trans. on Vehicular Technology*, 2021.
- [17] T. P. Weber and J. C. Gerdes, “Modeling and control for dynamic drifting trajectories,” *IEEE Trans. on Intelligent Vehicles*, 2023.
- [18] C. E. Garcia, D. M. Prett, and M. Morari, “Model predictive control: Theory and practice—a survey,” *Automatica*, 1989.
- [19] P. Riekert and T.-E. Schunck, “Zur fahrmechanik des gummibereiften kraftfahrzeugs,” *Ingénieur-Archiv*, 1940.
- [20] E. Fiala, “Seitenkraften am rollenden luftreifen,” *VDI*, 1954.
- [21] L. Ljung, “System identification.” Springer, 1998.
- [22] O. Dikici, E. Ghignone, C. Hu, N. Baumann, L. Xie, A. Carron, M. Magno, and M. Corno, “Learning-based on-track system identification for scaled autonomous racing in under a minute,” *IEEE Robotics and Automation Letters*, 2025.
- [23] A. Jain, M. O’Kelly, P. Chaudhari, and M. Morari, “BayesRace: Learning to race autonomously using prior experience,” in *Conference on Robot Learning*. PMLR, 2021.
- [24] J. L. Proctor, S. L. Brunton, and J. N. Kutz, “Generalizing koopman theory to allow for inputs and control,” *J. on Applied Dyn. Sys.*, 2018.
- [25] E. Perez, F. Strub, H. De Vries, V. Dumoulin, and A. Courville, “Film: Visual reasoning with a general conditioning layer,” in *AAAI*, 2018.
- [26] C. Chi, Z. Xu, S. Feng, E. Cousineau, Y. Du, B. Burchfiel, R. Tedrake, and S. Song, “Diffusion policy: Visuomotor policy learning via action diffusion,” *International Journal of Robotics Research*, 2025.
- [27] J. Snoek, O. Rippel, K. Swersky, R. Kiros, N. Satish, N. Sundaram, M. Patwary, M. Prabhat, and R. Adams, “Scalable bayesian optimization using deep neural networks,” in *Int. Conf. on Mach. Learning*, 2015.
- [28] J. Harrison, A. Sharma, and M. Pavone, “Meta-learning priors for efficient online bayesian regression,” in *International Workshop on the Algorithmic Foundations of Robotics*. Springer, 2018.
- [29] J. Watson, J. A. Lin, P. Klink, J. Pajarinen, and J. Peters, “Latent derivative Bayesian last layer networks,” in *AISTATS*, 2021.
- [30] F. Fiedler and S. Lucia, “Improved uncertainty quantification for neural networks with Bayesian last layer,” *IEEE Access*, 2023.
- [31] A. Davydov, F. Djeumou, M. Greiff, M. Suminaka, M. Thompson, J. Subosits, and T. Lew, “First, learn what you don’t know: Active information gathering for driving at the limits of handling,” *IEEE Robotics and Automation Letters*, 2025.
- [32] J. Levy, J. Gibson, B. Vlahov, E. Tevere, E. Theodorou, D. Fridovich-Keil, and P. Spieler, “Meta-learning online dynamics model adaptation in off-road autonomous driving,” *arXiv:2504.16923*, 2025.
- [33] J. Harrison, J. Willes, and J. Snoek, “Variational bayesian last layers,” in *International Conference on Learning Representations*, 2024.
- [34] P. Brunzema, M. Jordahn, J. Willes, S. Trimpe, J. Snoek, and J. Harrison, “Bayesian optimization via continual variational last layer training,” in *International Conference on Learning Representation*, 2025.
- [35] M. Bojarski, D. Del Testa, D. Dworakowski, B. Firner, B. Flepp, P. Goyal, L. D. Jackel, M. Monfort, U. Muller, J. Zhang *et al.*, “End to end learning for self-driving cars,” *arXiv:1604.07316*, 2016.
- [36] P. Cai, H. Wang, H. Huang, Y. Liu, and M. Liu, “Vision-based autonomous car racing using deep imitative reinforcement learning,” *IEEE Robotics and Automation Letters*, 2021.
- [37] B. Balaji, S. Mallya, S. Genc, S. Gupta, L. Dirac, V. Khare, G. Roy, T. Sun, Y. Tao, B. Townsend *et al.*, “Deepracer: Educational autonomous racing platform for experimentation with sim2real reinforcement learning,” *arXiv:1911.01562*, 2019.
- [38] P. Drews, G. Williams, B. Goldfain, E. A. Theodorou, and J. M. Rehg, “Aggressive deep driving: Model predictive control with a cnn cost model,” *arXiv preprint arXiv:1707.05303*, 2017.
- [39] X. Xiao, T. Zhang, K. Choromanski, E. Lee, A. Francis, J. Varley, S. Tu, S. Singh, P. Xu, F. Xia *et al.*, “Learning model predictive controllers with real-time attention for real-world navigation,” *arXiv preprint arXiv:2209.10780*, 2022.
- [40] E. Adabag, M. Greiff, J. Subosits, and T. Lew, “Differentiable model predictive control on the gpu,” *arXiv preprint arXiv:2510.06179*, 2025.
- [41] E. S. Lupu, F. Xie, J. A. Preiss, J. Alindogan, M. Anderson, and S.-J. Chung, “MAGIC vfm-meta-learning adaptation for ground interaction control with visual foundation models,” *IEEE Trans. on Robotics*, 2024.
- [42] P. Roth, J. Frey, C. Cadena, and M. Hutter, “Learned perceptive forward dynamics model for safe and platform-aware robotic navigation,” *arXiv:2504.19322*, 2025.
- [43] M. P. Deisenroth and C. E. Rasmussen, “Pilco: A model-based and data-efficient approach to policy search,” in *ICML*, 2011.
- [44] J. Harrison, J. Willes, and J. Snoek, “Variational bayesian last layers,” in *International Conference on Learning Representations*, 2024.
- [45] Y. Fu, M. Lou, and Y. Yu, “Segman: Omni-scale context modeling with state space models and local attention for semantic segmentation,” in *Computer Vision and Pattern Recognition Conference*, 2025.
- [46] M.-H. Guo, C.-Z. Lu, Q. Hou, Z. Liu, M.-M. Cheng, and S.-M. Hu, “Segnext: Rethinking convolutional attention design for semantic segmentation,” *Neural Information Processing Systems*, vol. 35, 2022.
- [47] E. Xie, W. Wang, Z. Yu, A. Anandkumar, J. M. Alvarez, and P. Luo, “SegFormer: Simple and efficient design for semantic segmentation with transformers,” *Neural Information Processing Systems*, 2021.

- [48] P. Mortimer, R. Hagmanns, M. Granero, T. Luettel, J. Petereit, and H.-J. Wuensche, “The goose dataset for perception in unstructured environments,” in *Int. Conference on Robotics and Automation*, 2024.
- [49] S. Hochreiter and J. Schmidhuber, “Long short-term memory,” *Neural Computation*, 1997.
- [50] L. Xuhong, Y. Grandvalet, and F. Davoine, “Explicit inductive bias for transfer learning with convolutional networks,” in *International Conference on Machine Learning*. PMLR, 2018.
- [51] J. Nocedal and S. J. Wright, *Numerical optimization*. Springer, 2006.
- [52] B. Stellato, G. Banjac, P. Goulart, A. Bemporad, and S. Boyd, “Osqp: An operator splitting solver for quadratic programs,” *Mathematical Programming Computation*, 2020.
- [53] OxTS, “User manual: NCOM data format for the efficient communication of navigation measurements,” 2022.
- [54] L. V. Labs, “Triton 3.2 mp technical reference manual,” 2025. [Online]. Available: <https://support.thinklucid.com/triton-tri032s/>
- [55] I. Loshchilov and F. Hutter, “Decoupled weight decay regularization,” in *International Conference on Learning Representations*, 2019.